Recent developments in shadow imaging prediction

David G. Sheppard
Dennis M. Douglas
Bobby R. Hunt
Integrity Applications Incorporated, 535 Lipoa Parkway, Suite 101, Kihei, Hawaii, USA

ABSTRACT

Shadow imaging is a technique to obtain highly resolved silhouettes of resident space objects (RSOs) which would otherwise be unattainable using conventional terrestrial based imaging approaches. This is done by post processing the measured irradiance pattern (shadow) cast onto the Earth as the RSO occults a star. The research presented here focuses on recent developments in shadow imaging of geosynchronous (GEO) satellites with near stationary orbits approximately 36,000 km from the Earth. Building upon previous results, validation testing of a high fidelity shadow prediction tool will be presented using data collected by small aperture Raven class telescopes. The solution space for optimal placement of one or more shadow imaging sensor systems will be explored based on a global population of GEO satellites over a one year time frame. These results will be based on the morphology of shadow densities on the Earth and on the solution of a constrained optimization problem.

1. INTRODUCTION

Geosynchronous (GEO) satellites perform many functions from their location at a nominal altitude of 36,000 km. At this altitude, even the largest terrestrial based optical telescopes are only capable of capturing imagery with resolvable features of several meters on GEO satellites. There is a growing need to observe the GEO belt with better resolution. Shadow imaging of GEO satellites as they occult (or pass in front of) distant bright stars offers a means of recovering fine resolution silhouettes which contain information about satellite antennae and solar panel configuration, satellite pose, and the presence of other space objects in close proximity.

Historically, shadow observation using a single collection aperture was first proposed in 1952 by Taylor [1], and a shadow of the asteroid Pallas was first successfully observed in 1978 [2]. Techniques have been developed to study distant objects in the Kuiper Belt and Oort Cloud using serendipitous observations of stellar occultations [3]. The idea of shadow imaging of GEO satellites using a linear array of small collection apertures coupled to high speed detectors was first proposed in 2005 by Burns, et al., [4], and further examined by Luu, et al., [5], and Paxman [12]. Work by Douglas in 2014 examined the image resolution limits of shadow imaging using a radiometric-based wave optics simulation approach by varying environmental, observational, and light collection parameters [6]. Recent work by Douglas, et al., has concentrated on examining shadow imaging modeling and simulation and image reconstruction algorithm performance [7][8][9][11].

In shadow imaging, it is important to calculate where to locate a terrestrial-based observer to capture the shadow as it traverses the earth, or in other words "be in the right place, at the right time." Development and refinement of a GEO satellite shadow prediction calculator is the focus of this paper. In the following subsections, an overview of the methodology for prediction is presented, and recent progress is presented in the following areas: (1) the predication accuracy of the current tools is examined using astrometric data from the USAF Raven small telescopes; and (2) the problem of global optimal shadow imaging sensor location is explored using a large population of GEO satellites.

2. SHADOW PREDICTION EXPERIMENTS

2.1 Shadow Location Prediction

In this section, we review the methods used for predicting the shadow location on the earth. The methods rely mainly on geometry, although the earth atmosphere introduces randomness due to atmospheric refraction. Successful shadow imaging prediction requires accuracy on the order of tens of meters in predicting where a shadow track will pass on the Earth. This translates into a requirement on angular precision of satellite and stellar positions of approximately 100 mas. This has also been discussed in prior publications [7][8][9][10].

2.1.1 Stellar Astrometrics

The choice of star catalog is important since not all contain the same levels of positional accuracy. The second data release from the Gaia mission, called Gaia DR2, includes an astrometric solution for over 1.6 billion stars. The accuracy is unprecedented, being on the order of 200 micro arc seconds, and will become more accurate as the Gaia mission proceeds to its conclusion. With the Gaia DR2, and following, the main remaining source of uncertainty in shadow imaging prediction is in the satellite position. In our work, the satellite positions are compared to stellar astrometric positions at the epoch of interest in either an inertial or terrestrial frame using the IAU Standards of Fundamental Astronomy software [17].

2.1.2 Satellite Position Calculations

The position of a satellite is typically computed using a Two Line Element (TLE) set coupled with the SGP4 theory as discussed in Vallado [14]. The accuracy of satellite state predictions based on TLE data has been the subject of prior study [15], where GEO satellites orbital position errors were reported to be on the order of hundreds of meters or more at the TLE epoch. In Section 2.2.1, we present some results related to the cross-track orbital position errors that can be encountered when using TLE data.

2.1.3 Earth Ellipsoid Intersection and Refraction Correction

An algorithm by Pucinelli [13] is the basis for locating the sensor boresight pointing to a first approximation (without atmospheric refraction). The algorithm poses the problem as the solution to a quadratic equation and provides both the near and far intersections. Refraction due to the earth atmosphere causes the shadow to be displaced from this idealized location, and is particularly difficult to deal with at zenith angles greater than 70 degrees. In our work, we confine our studies to zenith angles less than 70 degrees where it is reasonable to pursue a one-step geometric solution based on a fixed height atmosphere.

2.2 Results and Discussion

In this section, we summarize progress achieved thus far in testing the tools needed to predict the location of a shadow on the earth at large scales. The testing was done using data from the Raven small telescope systems located at Kihei, Maui. We also present examples of the distribution of shadows on the earth at small map scales for a large global population of GEO satellites and indicate optimal sensor locations for this population.

2.2.1 Shadow Prediction Tests with Raven Data

The Raven small telescope systems located on Maui at the Remote Maui Experiment facility (location: 20.7463 156.4317 W) collect a large amount of imagery. A data mining algorithm was applied to search through the astrometric results for imagery in which the observed space object would pass close to one of the stars in the field of view. Several observations of the Galaxy15 and TDRS 5 satellites during 2016 and 2017 were identified meeting this criterion. The astrometric data associated with these observations were compared to past-predictions based on the tasking TLE used by the Raven system for each observation. The Gaia DR2 catalog was used for stellar positions. The following table shows information for the satellites used in the study taken from the Space-Track Geostationary Report [20].

Table 1. Galaxy15 and TDRS5 data

Satellite	NORAD ID	Inclination	Apogee (km)	Perigee (km)	Longitude
Galaxy 15	28884	0.05°	35795	35777	133° W
TDRS 5	21639	14.31°	35891	35678	166.9° W

The computation of an astrometric plate solution using the stars in the field of view is basic to the calibration of each Raven image. This permits measurement of the observed locations of the satellite and the star and the derivation of a computed shadow location predicted by the astrometric image processing. These positions were then compared with those predicted by SGP4/SDP4 propagations and catalog star positions. The right ascension and declination of the satellite as measured on the Raven focal plane was mapped to a ground location using the geometry of a line intersecting an ellipsoid of rotation. These calculations were done using Vallado's coordinate transformations in Matlab [19]. Previous work has shown that the Vallado propagation and coordinate transforms as implemented in Matlab and those in the Orekit 8.0 library [18] agree very closely. All coding was done in Matlab.

The data set used to produce the results below consists of 257 FITS images and their corresponding Astrograph AST files, after removal of outliers corresponding to defective TLE data. In some cases, there are multiple observations of the satellite during the same night. We have not excluded these additional observations from the data set since in many cases they involve the satellite approaching a different star during the night. Even so, it is clear from the results that the TLE data introduces significant errors in the predicted shadow locations. Fig. 1 shows the shadow location results decomposed into North-South and East-West errors and plotted versus observation number. Fig. 2 shows the same data as histograms. In these plots, we do not distinguish between the two satellites. For GEO satellites, shadow tracks follow a West-to-East trajectory on Earth and are nearly parallel to the equator. The greater the orbital inclination, the more tilted the shadow track. From an operational standpoint, the N-S errors are much more important in trying to position a shadow imaging system. The E-W errors mainly affect the timing of the occultation event, but do become important at larger orbital inclinations.

The satellite N-S displacement errors on orbit are closely related to cross-track error, particularly for Galaxy 15 with its low orbital inclination. They are computed from the shadow's latitude error using a straightforward geometric projection based on the observed elevation of the satellite. Fig. 3 displays the detailed plots of the satellite on orbit N-S displacements. The uncertainties associated with the N-S orbital position are generally in agreement with Flohrer [15], who examined satellite positional accuracy at the TLE epoch, while the typical time from epoch of a tasking TLE used by a Raven system is approximately one day. Table 2 summarizes the first and second order statistics for the prediction errors across this data set.

From these results, it should be clear that TLE accuracy is not sufficient to support the requirements of a shadow imaging system. Much more accurate orbital data will be necessary.

Table 2. First and second order statistics for shadow and satellite displacement errors (units: km)

Satellite	# Obs	μ_{ns}	σ_{ns}	$\mu_{sat\ ns}$	$\sigma_{sat\ ns}$
Galaxy 15	50	0.7659	0.7735	0.6198	0.6259
TDRS 5	207	-1.3374	0.6586	-1.2535	0.5912

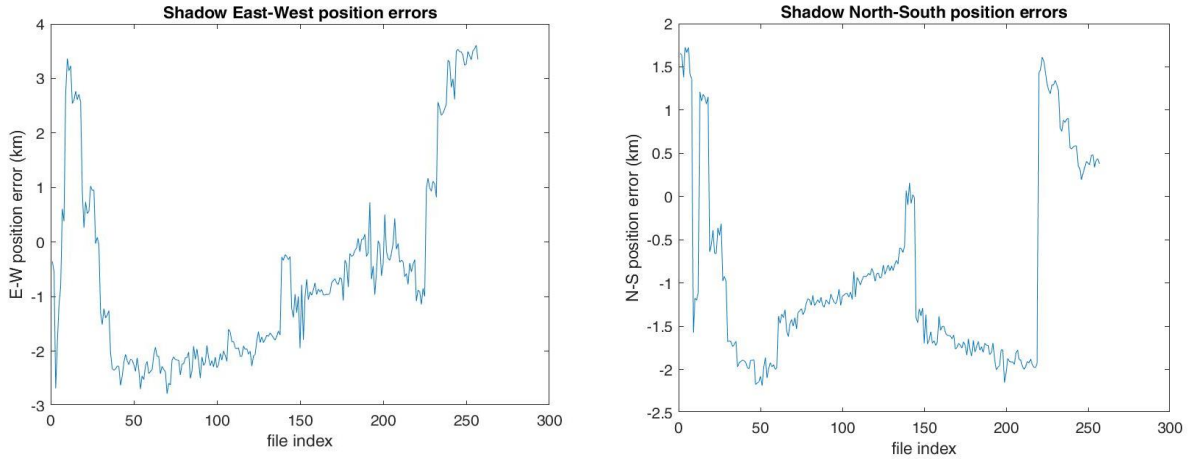

Fig. 1. Positional errors between shadow locations predicted using the SGP4/SDP4 propagator and Astrograph image processing: (left) E-W errors; (right) N-S errors. File index refers to the Astrograph file.

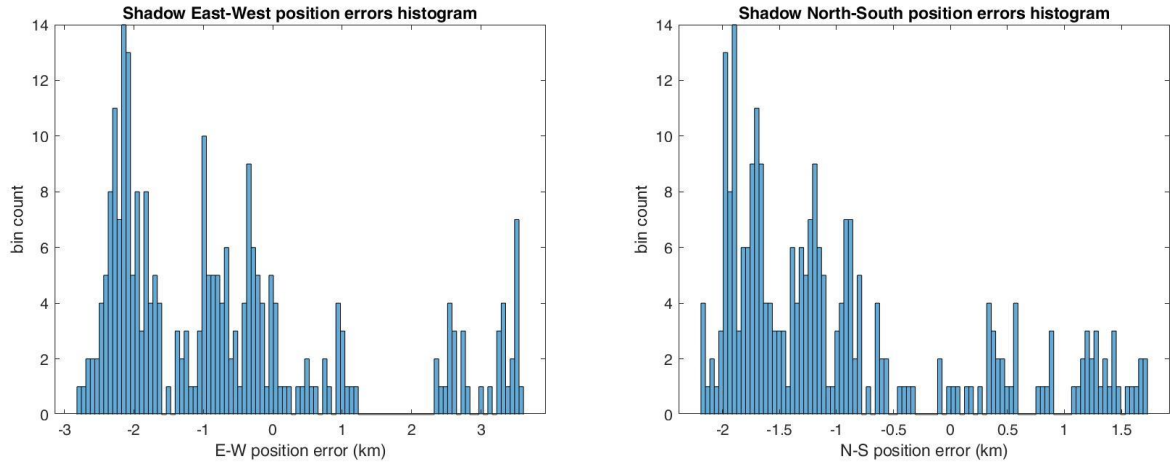

Fig. 2. Positional errors between shadow locations predicted using the SGP4/SDP4 propagator and Astrograph image processing (left) E-W errors; and (right) N-S errors. Histograms have 100 bins.

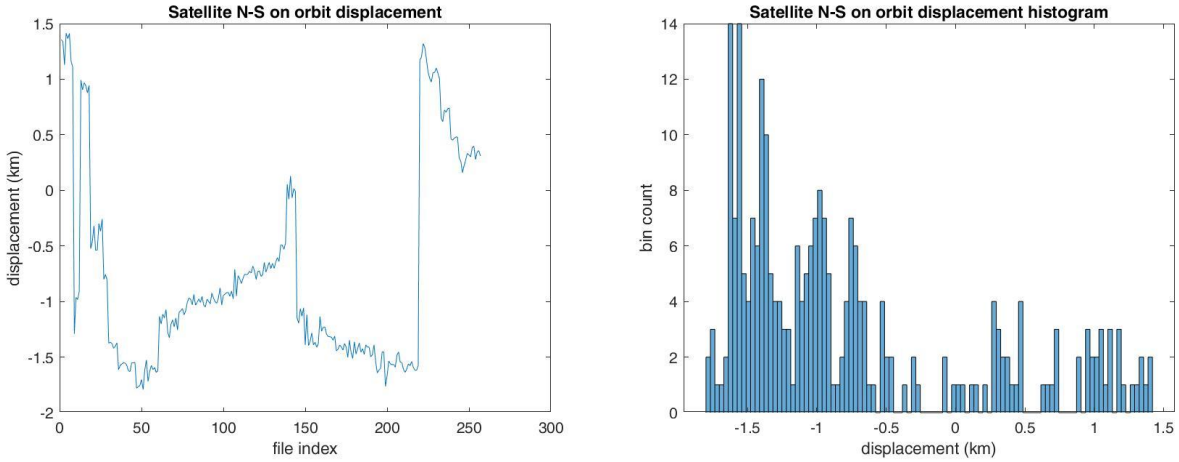

Fig. 3. On orbit N-S displacements of the satellites: (left) plotted versus observation number; and (right) plotted as a histogram with 100 bins.

2.2.2 Sensor Location using Small Scale Shadow Density Morphology

The capability to map the density of shadows produced by one or more satellites at small scales is important to the sensor placement problem. In this section, we examine this problem using a population of 315 real GEO satellites taken from the Space-Track GEO Report [20]. Although the report lists more than 800 satellites, this study is limited to a population to satellites with a fairly complete set TLE data for 2015. The distribution of this population is somewhat biased toward the USA and Europe, as can be seen in Fig. 4. Although one could seek to use a more evenly distributed population, it is a certainty that any real population of interest, e.g. those belonging to a particular country, will exhibit similar tendencies. This bias is quite apparent later on in its effect on the global shadow cost map.

This study incorporates heuristic cost functions to weight the shadow density map in ways that support better image reconstruction, which is a function of observer zenith angle and the brightness of the occulted star. Fig. 5 shows the cost functions applied in computing the map. The functional forms are derived from the Signal-to-Noise results reported by Douglas [6]. Shadow imaging reconstruction is robust across a wide range of zenith angles and stellar magnitudes, and this is reflected in the cost functions. The functions are applied by taking the contribution of each shadow cast by a satellite to each bin of the shadow density map and multiplying by the cumulative product of the

cost functions evaluated at that shadow location. By incorporating cost functions, the shadow density map represents a brute force grid search approach to solving the constrained optimal sensor location problem.

The resulting cost function surface map is shown in Fig. 6. The surface of the earth is binned into 1 degree by 1 degree quadrangles to produce a cost map of shadow density on the Earth surface. The map was generated for the year 2015, and was composed of maps computed once every ten days. Additionally, the following considerations were applied:

- Sensor locations were constrained to lie within a range of latitudes in [-55,55]
- Illumination at the shadow location was constrained to nautical night time
- The cost map was smoothed by convolution with a Gaussian kernel ($\sigma = 2$)

Fig. 7 shows horizontal and vertical slices through the map at the location of the maximum value. The vertical slice shows that the maximum is fairly broad at its peak, implying that there is considerable flexibility in the latitude location of the system. The horizontal slice shows a stronger preference for a particular longitude. Lastly, Fig. 8 shows a Google Earth depiction of the location of the maximum value of the cost map. The location is in Northeastern Ethiopia near the border with Djibouti.

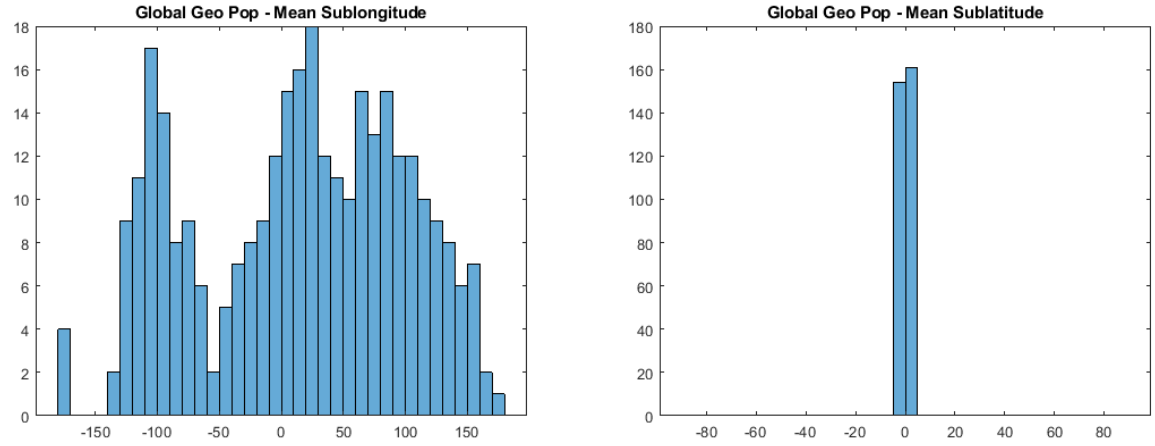

Fig. 4. Sublongitude and Sublatitude population distribution

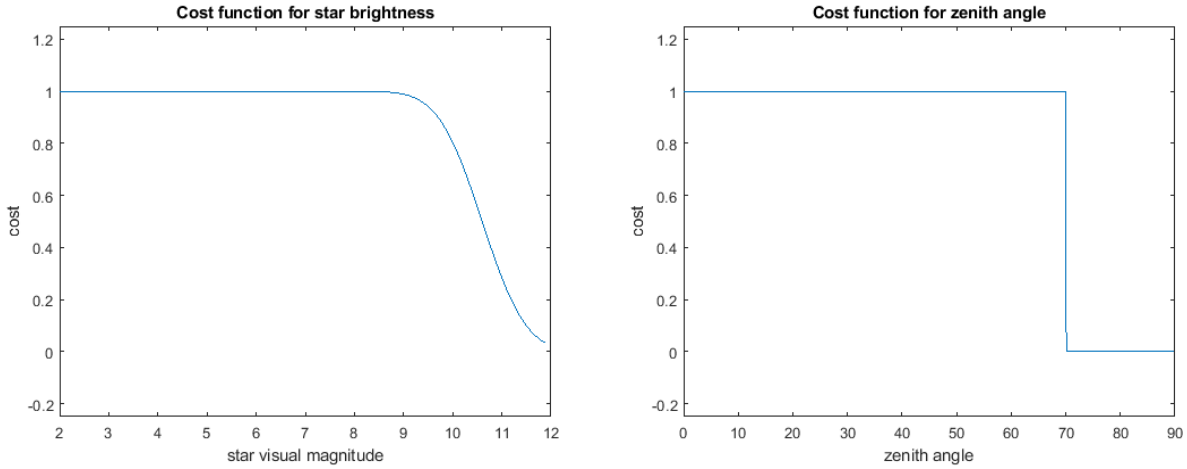

Fig. 5. Cost functions used to weight map contributions

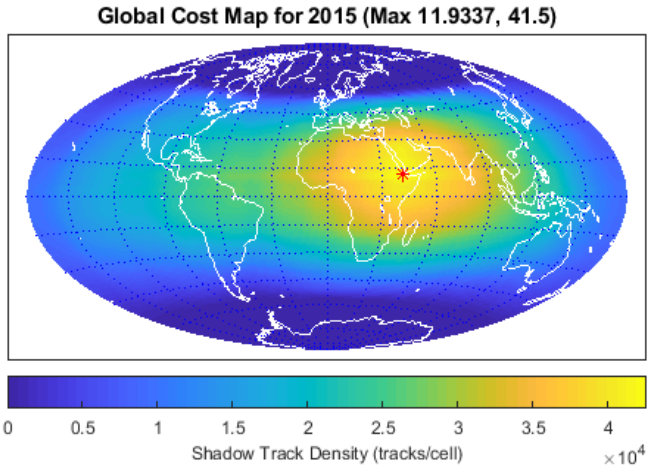

Fig. 6. Depiction of cost-function weighted global shadow density for 315 GEO satellites. (The maximum is denoted by the asterisk.)

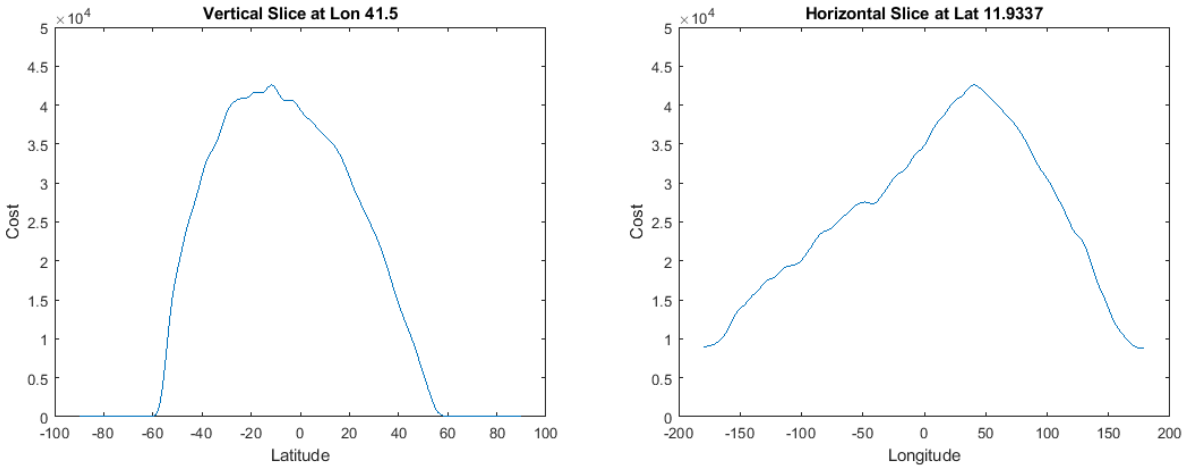

Fig. 7. Slices through the maximum of the cost map.

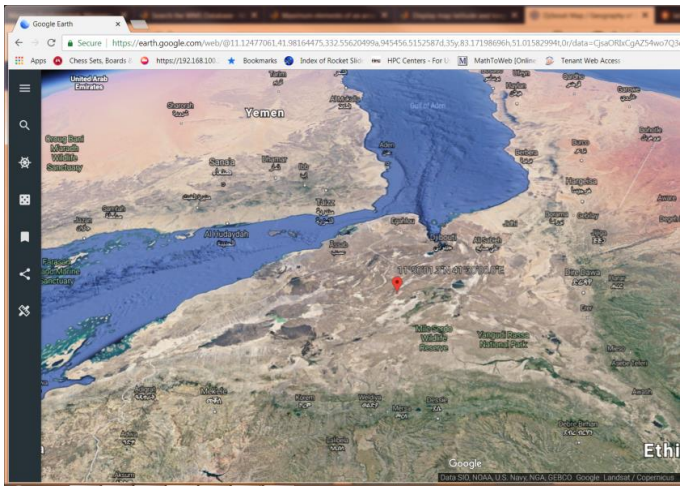

Fig. 8. Optimal location shown using Google Earth (Ethiopia/Djibouti border)

3. CONCLUDING REMARKS

The foregoing has reported on progress that our group has made in developing the tools needed to characterize the accuracy of shadow locations predicted using TLE data, as well as exploring the solution space for the optimization of sensor placement using a real satellite population. The inadequacy of TLE data in supporting shadow imaging prediction was demonstrated. Future work may include the following: (1) determining optimal sensor locations for specific satellite populations of concern; (2) seeking additional opportunities to work with real data and to collect successfully an actual GEO satellite occultation event in real time; and (3) characterizing shadow imaging prediction with more accurate orbit data.

4. ACKNOWLEDGEMENTS

This work was supported by the United States Air Force Office of Scientific Research (AFOSR) grant FA9550-15-C-0035 and managed by Dr. Stacie Williams. We would also like to thank Paul Sydney for his support in enhancing Astrograph image processing with additional features intended to support the data mining.

5. REFERENCES

[1] G. E. Taylor, "An occultation by a minor planet," Astronomical Society of South Africa 11 (1952).
[2] L. Wasserman, R. L. Millis, O. G. Franz, E. Bowell, and N. M. White "An occultation by a minor planet," *Astronomical Journal* **84** (1979).
[3] F. Roques, G. Georgevits, and A. Doressoundiram, "The Kuiper Belt Explored by Serendipitous Stellar Occultations," in *The Solar System Beyond Neptune*, Barucci, M. A., Boehnhardt, H., Cruikshank, D. P. and Morbidelli, A. (eds.), University of Arizona Press, Tucson, pp. 545-556 (2008).
[4] R. H. Burns, V. Gamiz, J. J. Dolne, J. Lambert, and S. Long, "Shadow Imaging of GEO Satellites," *Proc. SPIE* **5896** (2005).
[5] J. Luu, L. Jiang, and B. Willard, "Shadow imaging efforts at MIT Lincoln Laboratory," *Proc. AMOS Technical Conference, Wailea, Maui, Hawaii* (2008).
[6] D. M. Douglas, "Shadow Imaging of Geosynchronous Satellites," Ph.D. Dissertation, University of Arizona, Tucson (2014).
[7] D. M. Douglas, B. R. Hunt, and D. G. Sheppard, "Shadow imaging of geosynchronous satellites: simulation, image reconstruction, and shadow prediction," *Proc. SPIE* **9982** (2016).
[8] D. Douglas, B. R. Hunt, and D. Sheppard, "Recent Developments in Shadow Imaging of Geosynchronous Satellites," *Proc. AMOS Technologies Conference, Wailea, Maui, Hawaii* (2016).
[9] D. M. Douglas, B. R. Hunt, and D. G. Sheppard, "Resolution limits for shadow imaging of geosynchronous satellites: analytic and simulated approaches," *Proc. SPIE* **10410** (2017).
[10] D. G. Sheppard, D. M. Douglas, B. R. Hunt, "Recent Developments in Shadow Imaging," *Proc. AMOS Technologies Conference, Wailea, Maui, Hawaii* (2017).
[11] D. Douglas, D. G. Sheppard, and B. R. Hunt, "Advances in shadow prediction of geosynchronous satellites," to appear in Proc. SPIE Optics and Photonics (2018).
[12] R. G. Paxman, "Synthetic-Aperture Silhouette Imaging (SASI)," *Proc. AMOS Technologies Conference, Wailea, Maui, Hawaii* (2016).
[13] Puccinelli, E. F., "Ground Location of Satellite Scanner Data," *Photogrammetric Engineering & Remote Sensing* **42**, 4, pp. 537-543 (1976).
[14] D. A. Vallado, *Fundamentals of Astrodynamics and Applications, 4th Edition*, Microcosm Press, Hawthorne, CA (2013).
[15] T. Flohrer, H. Krag, and H. Klinkrad, "Assessment and Categorization of TLE Orbit Errors for the US SSN Catalog," *Proc. AMOS Technologies Conference, Wailea, Maui, Hawaii* (2008).
[16] GAIA Data Release 2 (GAIA DR2) (available at https://cosmos.esa.int/web/gaia/dr2).
[17] International Astronomical Union Standards of Fundamental Astronomy (SOFA) (available at http://www.iausofa.org/).
[18] ORbits Extrapolation KIT (OreKit) (available at https://www.orekit.org/).
[19] Astrodynamics Software by D. Vallado (available at https://celestrak.com/software/vallado-sw.asp).
[20] Space-Track Geosynchronous Report (available at https://www.space-track.org).